2008

Effects of C substitution on the pinning mechanism of MgB2

Jianli Wang
University of Wollongong, jianli@uow.edu.au

Rong Zeng
University of Wollongong, rzeng@uow.edu.au

Jung Ho Kim
University of Wollongong, jhk@uow.edu.au

Lin Lu
University of Wollongong, ll972@uowmail.edu.au

S. X. Dou
University of Wollongong, shi@uow.edu.au

Effects of C substitution in MgB_2 on the pinning mechanism

J.L. Wang, R. Zeng, J.H. Kim, L. Lu and S.X. Dou

Institute for Superconducting and Electronic Materials, University of Wollongong, Northfields Avenue, Wollongong, NSW 2522, Australia

Abstract

The temperature and magnetic field of the critical current density of four selected pure and C-doped MgB_2 samples have been investigated in detail and the flux pinning mechanism has been analysized. It was found that the sintering temperature and the substitution of carbon can significantly modify the flux pinning mechanism. Below 30 K, the reduced field dependences of the reduced pinning force for all investigated samples are found to closely obey one scaling law, reflecting the presence of only one dominant pinning mechanism. A δT_c pinning mechanism was found to be mainly responsible in pure MgB_2 samples while the δl pinning mechanism becomes dominant for C-doped samples.

Key Words: MgB_2, Carbon substitution, flux pinning mechanism, Critical currents

PACS: 74.70.Ad , 74.25.-q, 74.25.Qt, 74.25.Op, 74.25.Sv

Introduction

The discovery of superconductivity in MgB_2 below 39 K has attracted a huge amount of attention [1-10] due to its great potential for applications and variety of unusual properties, such as its order parameter symmetry and the large anisotropy ratio of the upper critical field H_{c2}^{ab}/H_{c2}^{c} [2].

Because the strong pinning and high upper critical field are critical for many MgB_2 applications, a lot of efforts have been made to introduce dopants into the host structure to elucidate how the crystal structure, internal charge states, and T_c are interrelated, as well as how to improve the superconducting properties [2-6]. It was proved that the doping [10, 11] and particle irradiation [12] could be appropriate methods for improving the upper critical field H_{c2} and high field transport J_c of MgB_2 and carbon seems to be most promising for enhancing H_{c2} among the numerous possibilities of doping MgB_2 [3, 10]. Moreover, study of the vortex matter phase diagram of MgB_2 can help in understanding the pinning mechanism of this material. It is accepted that the flux pinning force density is a function of temperature and magnetic field [13] and is determined by the micro and nanostructure of the sample [10, 12, 14, 15]. The field dependence of normalized flux pinning force can give an indication of the pinning mechanism operative in the particular sample [8, 10, 12, 16]. According to the size of pinning center, the pinning mechanism can be classified into three types [14]: point, surface and volume. Grain boundary (surface type) is found to be the main pinning mechanism in MgB_2 samples [12, 16]. Recently, it also was found that the pinning mechanism can be modified by SiC-doping [15] and the neutron irradiation [16].

In type-II superconductors, it is accepted that there are two very important elementary interactions between vortices and pinning centers: the magnetic interaction and the core interaction [13]. The magnetic interaction stands for the interaction of surfaces between superconducting and non-superconducting materials parallel to the applied field

and is very small compared with the core interaction in MgB_2-based samples, due to its large GL coefficient κ (~26 in MgB_2 [7]). The core interaction stands for the coupling of the locally distorted superconducting properties with the periodic variation of the superconducting order parameter. The core interaction includes two types of mechanism: δT_c and δl pinning. The δT_c pinning refers to the spatial variation of the GL coefficient associated with disorder due to variation in the transition temperature T_c, while δl pinning is associated with the variation in the charge-carrier mean free path l near lattice defects [7, 13]. For polycrystalline [7], thin film [8], and single crystalline [9] MgB_2 samples, it has been found that the dominant pinning mechanism is δT_c pinning, which is related to spatial fluctuation of the transition temperature. However, it is unclear whether this is true with respect to the mechanism involved in C-doped MgB_2 samples, because C substitution for B in MgB_2 leads to further disorder [3] and an increase in the residual resistivity [10], reflecting the shortening of the mean free path l.

In this investigation, we will focus on these issues and try to understand the effects of sintering temperature and C substitution in MgB_2 on the physical properties, especially on the pinning mechanism.

Experimental process

MgB_2 bulk samples were prepared by an *in-situ* reaction method [3]. Powders of magnesium (Mg, 99%) and amorphous boron (B, 99%) were mixed for fabrication of MgB_2 bulks. The carbon-doped MgB_2 samples were obtained by combining the magnesium (Mg, 99%) and amorphous boron (B, 99%) powders with citric acid ($C_6H_8O_7$). All the samples were sealed in iron tubes, sintered in a tube furnace at 650°C to 950°C for 30 min in an argon atmosphere, and finally furnace-cooled to room temperature. In this investigation,

four samples prepared under different conditions were selected and labeled as Nos. 165 and 185 for pure MgB_2 and Nos. 485 and 495 for C-doped samples. The experimental details are described in Table I.

Results and discussion:

(1) Lattice parameters

All these four samples show almost identical x-ray diffraction patterns. Analysis of the x-ray diffraction patterns of randomly-oriented fine powder samples showed that all samples are essentially single phase and have the MgB_2 structure, as expected, with an amount of less than 10 wt% MgO constituting the single impurity phase. The x-ray data were analyzed by Rietveld refinement using the FULLPROF program [17]. Figure 1 shows the experimental and calculated x-ray diffraction patterns for sample No. 485 as a typical example. The pattern factor R_p, the weighted pattern factor R_{wp}, and the expected pattern factor R_{exp} are 5.41, 7.39, and 5.37, respectively. The results of the refinements for all compounds are listed in Table I. It can be seen that the carbon doping leads to an obviously anisotropic variation of the unit cell (c/a) with a larger decrease for the a-axis. The carbon content in the C-doped $Mg(B_{1-x}C_x)_2$ samples was estimated and is listed in Table I using $x = 7.5 \times \Delta(c/a)$, with $\Delta(c/a)$ being the change in c/a compared to the pure MgB_2 [11], as reported in [3]. (Here we use the single crystal MgB_2 as a reference point [18].)

(2) Flux pinning mechanism

We have measured the magnetic hysteresis loops (MHL) for all samples at various temperatures below T_c. From these $M(H)$ loops, the $J_c(B)$ curves at various temperatures have been calculated using the Bean model [3] and are shown in Fig. 2 (a) and (b) for samples No. 185 and 485, respectively, as typical examples. The case is quite similar for other two samples. The curves for lower temperature ($T < 13$ K) are not shown because of

large flux jumping. It can be seen that the C-doping sample exhibits higher J_c values compared with the undoped sample at the same sintering temperature. For example, J_c at 15 K and 20 K for No. 485 achieve 62000 A/cm^2 and 33000 A/cm^2 at 1 T, respectively, while the corresponding values are 44000 A/cm^2 and 29000 A/cm^2 for No. 185 by comparison.

It is well established that, in the mixed state of a type II superconductor, if the flux pinning is dominated by a single mechanism, the field dependence of the pinning force ($F_p = \mu_0 H \times J_c$) should obey the general relationship [8, 14] that F_p is proportional to $h^n(1-h)^m$, where h is the reduced field, with $h = H/H_{irr}$, and n and m depend on the type of pinning. There are various methods reported in the literature [8] to determine the irreversibility field $B_{irr} = \mu_0 H_{irr}$ in MgB_2, deriving it from both the magnetization and the resistivity. Here, we use the J_c criteria of 10^6 A/m^2 to determine the value of H_{irr} [7]. It was found that for all the samples investigated, the temperature dependence of $\mu_0 H_{irr}$ can be closely fitted using $\mu_0 H_{irr}(T) = \mu_0 H_{irr}(0)[1-(T/T_c)^2]^{3/2}$, which is characteristic of 3D flux creep [7, 8, 13]. The similar behavior of B_{irr} has been reported for MgB_2 thin film samples [8]. The experimental data for B_{irr} are shown with the fitting result in the insets of Fig. 2 for samples No. 185 and No. 485 as a typical example.

The pinning force F_p has been calculated using $F_p = \mu_0 H \times J_c$, and we plot the curves of the reduced pinning force f versus the reduced magnetic field h ($f = F_p/F_{p\,max}$ with $F_{p\,max}$ standing for the maximum of the pinning force, $h = H/H_{irr}$) in Figs. 3(a), (b), (c) and (d) for samples Nos. 165, 185, 485, and 495, respectively. It can be seen clearly that the f vs. h curves exhibit a scaling behavior similar to what is observed in thin film MgB_2 samples [8]. This reflects the fact that there is a single dominant pinning mechanism below 30 K in these samples. We have fitted the experimental data using the scaling law $h^n(1-h)^m$ and found that it works quite well below 30 K. The experimental data and fitting results (shown as a

solid line) are shown in Figs. 3(a), (b), (c) and (d) with corresponding parameters. We note that sample No. 165 gives a quite different value of n and m (with n = 1.03 and m = 2.96) compared with the other three samples, where n is around 0.60 (n = 0.61, 0.60, and 0.60 for Nos. 185, 485, and 495, respectively) and $m \approx 2.0$ (m = 1.81, 1.87, and 2.08 for Nos. 185, 485, and 495, respectively). It has been well established that when n is close to 0.5 (with $m \approx 2$), the grain boundary pinning plays a major role [14], while the non-superconducting point centers becomes mainly responsible with n = 1. This means that grain boundary pinning is the overriding pinning mechanism for samples Nos. 185, 485, and 495 (n ~0.6) (similar case has been observed in [14] for SiC-doping MgB_2 samples and undoped MgB_2 samples with poor J_C values at low magnetic field) while the point pinning becomes dominant in sample No. 165 where n is close to 1 (similar case observed in [8] for MgB_2 thin films deposited by sputtering and in [14] for the undoped samples with high *Jc* values at low magnetic field). The fact that the exponent m in No. 165 is larger than 2 expected for conventional superconductors [14] can be understood in terms of a possible distribution of parameters determining F_p combined with the particular choice of H_{irr} [19] and the similar case has been observed for $YBa_2Cu_3O_7$ thin films [19] with inhomogeneity and undoped MgB_2 [15]. The variation in the pinning mechanism from samples 165 to 185, 485, and 495 can be understood in terms of the crystallinity. Compared with the No. 165 sample, samples Nos. 185, 485, and 495 were sintered at rather higher temperatures (850 and 950 °C) and will show an improvement in the crystallinity, leading to fewer point defects within the samples. Moreover, one finds that the fitting of $F_{p\,max}$ against H_{irr} gives a similar value of α using $F_{p\,max} \propto H_{irr}^{\alpha}$ ($\alpha \approx 1.71$, 1.61, 1.75, and 1.71 for samples Nos. 165, 185, 485, and 495, respectively). The fitting results are shown as the insets of Figs. 3. From Figs. 3, it also can be found that the peak of the experimental f_p curves at lower temperatures

takes place around 0.2 for the samples No. 185, 485 and 495 while it slightly shifts to around 0.25 for No. 165 sample reflecting the variation of pinning defect center density. The f_p curves for No. 165 are much narrower compared with other three samples.

It is accepted that the critical current density J_c is determined by the pinning force and can act a suitable parameter to check the validity of the collective pinning theory with the experimental results [13]. According to the collective pinning model, the disorder-induced spatial fluctuations in the vortex lattice can be clearly divided into markedly different regimes according to the strength of the applied field: single-vortex, small-bundle, large-bundle, and charge-density-wave (CDW)-type relaxation of the vortex lattice [13]. With the applied field below the first critical field B_{sb} (where B_{sb} stands for the crossover field from the single vortex regime into small bundles of vortices), the interaction between the vortices is irrelevant, and J_c is independent of the field. Within the intermediate field range $B_{sb} < B < B_{lb}$ (with B_{lb} standing for the crossover field from small-bundle to large-bundle pinning), the dispersion in the elastic modulus becomes relevant, and J_c will decrease exponentially (in the small-bundle range). In the large-bundle pinning range, the field of J_c turns algebraic with B ($J_c \propto B^{-3}$) [7]. B_{sb} in [13] has been defined as

$$B_{sb} = \beta_{sb} \frac{j_{sv}}{j_0} H_{c2} \tag{1}$$

where β_{sb} can be regarded as constants (as within the framework of the dynamical approach $\beta_{sb} \approx 5$) [13]. J_0, H_{c2} ($H_{c2} = \mu_0\Phi_0/\pi\xi^2$ where $\Phi_0 = h/2e$ is the flux quantum), and J_{sv} stand for the depairing current, the upper critical field and the critical current density in the single vortex-pinning regime, respectively. Using the $J_0 = 4B_c/3\sqrt{6}\mu_0\lambda$ and $B_c = \Phi_0/2\sqrt{2}\pi\lambda\xi$ [13], one can easily obtain:

$$B_{sb} = 3\sqrt{3}/2 \frac{\beta_{sb}\mu_0^2\lambda^2 j_{sv}}{\zeta} \tag{2}$$

It can be seen from Fig. 2 that, similarly to previous results [7] and in good agreement with the collective model [13], the J_c-B curve can be divided into three different regimes within our field range. In the small field regime, the J_c is almost independent of the applied field before it starts to decrease first exponentially and then algebraically with increasing field. In order to derive the value of B_{sb}, we plot the double logarithmic plot $-\log_{10}(J_c/J_c(B = 0))$ vs. B as shown in Fig. 4 using the data in Fig. 2 (b) for sample No. 485 as a typical sample. One can directly derive the value of the critical field B_{sb} at the departure point from the straight line (exponential dependence on field) in the intermediate field and likewise B_{th} (where B_{th} is the crossover field to the thermal fluctuations dominated regime), as shown in the insert of Fig. 4 for T=23 K. It is accepted that for δT_c pinning and δl pinning, the disorder parameter δ exhibits different characteristic temperatures [13]. Griessen et al. [20] have provided individual expressions of J_{sv} for δT_c pinning ($J_{sv} \propto (1\text{-}t^2)^{7/6}(1+t^2)^{5/6}$) and δl pinning ($J_{sv} \propto (1\text{-}t^2)^{5/2}(1+t^2)^{-1/2}$) contributions, so using these results, Qin et al. [7] obtained an expression for B_{sb} for the δT_c pinning and δl pinning cases, respectively, as follows:

$$B_{sb} = B_{sb}(0)\left(\frac{1-t^2}{1+t^2}\right)^{2/3} \tag{3}$$

and

$$B_{sb} = B_{sb}(0)\left(\frac{1-t^2}{1+t^2}\right)^{2} \tag{4}$$

Given the presence of core pinning in our samples, it is important to distinguish between the case of δT_c pinning and δl pinning for our investigated samples. We have used the equations (3) and (4) to fit our samples, and the results are shown in Figs. 5(a), (b), (c) and (d) for sample Nos. 165, 185, 485 and 495, respectively. It can be seen from Figs. 5 that for a pure MgB_2 sample the δT_c pinning is mainly responsible, while in the C-doped samples

the δl pinning becomes the dominant factor. In order to confirm this conclusion for the C-doped samples, we also have derived the temperature dependence of J_c at a particular field, as performed in [21] (here we use B = 0.1 T within the single vortex regime), and plotted $J_c(B$=0.1 T) vs. T as the inset of Figs. 5. Based on the fact that for δT_c pinning the disorder parameter δ is proportional to the ξ, while it changes into $\delta \propto \xi^{-3}$ for δl pinning, the theoretical different temperature dependences of $J_c(H,T)$ have been derived [21] as

$$j_c(t)/j_c(0) = (1-t^2)^{5/2}(1+t^2)^{-1/2} \quad (5)$$

for δl pinning and

$$j_c(t)/j_c(0) = (1-t^2)^{7/6}(1+t^2)^{5/6} \quad (6)$$

for δT_c pinning, respectively. We fit our experimental data using equations (5) and (6), respectively, as shown in the insets of Fig. 5. It can be seen that the δl pinning curve is in good agreement with the experimental data for the C-doped samples. This again supports the conclusion that for the C-doped samples the δl pinning plays a major role. A similar conclusion was also reached by Ohmichi et al. from studying the rf penetration depth of carbon-substituted MgB_2 single crystals [22].

In order to understand the different behaviors in the pure MgB_2 and C-doped samples, we also measured the transports for these four samples and the zero field results are shown in Fig. 6 as an example. We estimated the electronic mean-free path at T_c from the corrected residual resistivity ρ_0 for these four samples (listed in Table I) by using an average Fermi velocity of v_F =4.8 $\times 10^5$m/s and a carrier density of 6.7 $\times$ 10^{22} e/cm^3 [23]. According to Rowell, the corrected residual resistivity is defined as $\rho_0=\rho_{measure}(40K)\Delta\rho_{ideal}/\Delta\rho_{measure}$ where $\Delta\rho=\rho_{measure}(300K)-\rho_{measure}(40K))$ and $\Delta\rho_{ideal}$ is the corresponding value for pure single crystal of good quality and to be 4.3 $\mu\Omega$cm [24]. Here

we simple use the same carrier density for all samples as in the pure MgB_2 (two free electrons per unit cell) based on the fact that the carbon content roughly estimated here (see Table I) is less than 5% and the variation in carrier density (carbon has one more electron than boron) for carbon-substituted sample is less than 5% [25] which does not in practice affect the conclusion on the variation of free path and the accurate analysis is outside of our interest here. Moreover, it can be seen that higher temperature sintering can improve the connectivity (defined as $K=\Delta\rho_{ideal}/\Delta\rho_{measure}$) from 0.062 for No. 165 sample to 0.126 for No. 185 while the C-doping leads to a decrease in K (K =0.039 for sample No. 485).

From the transport measurements at various fields, we have derived the value of H_{c2} (at 10% of the resistance at zero field). Because the Werthamer-Helfand-Hohenberg (WHH) prediction ($H_{c2}(T = 0) = 0.7\ T_c\ dH_{c2}(T = T_c)/dT$) underestimates H_{c2} at low temperatures [26] for MgB_2-based samples, here we have derived H_{c2} at 0K to be 25.5 T, 26.3, 31.7 T, and 34.3 T using linear extrapolation of the low temperature data part of the $H_{c2}(T)$ vs. T dependence for sample Nos. 165, 185, 485 and No 495, respectively. (It has been reported that this method can provide a reasonable value of $H_{c2}(0)$ [26].) Using the equation $\xi = (\Phi_0/2\pi H_{c2})^{1/2}$, the values of $\xi(0)$ have been estimated and are listed in Table I.

Conclusion

We have investigated the magnetic and transport behavior of pure and C-doped MgB_2 samples. A low sintering temperature leads to more point defects, which is reflected by the presence of point pinning, while the grain boundary pinning mechanism becomes dominant for the samples with higher sintering temperatures. Moreover, it has been found that in the pure MgB_2 samples the δT_c pinning is dominant, while δl plays a major role for the C-doped samples.

Acknowledgement

This work was supported by the Australian Research Council, Hyper Tech Research Inc, and CMS Alphatech International Ltd. We thank Dr. Sangjun Oh for critical reading of the manuscript.

References:

[1] C. Buzea and T. Yamashita, Supercond. Sci. Technol. **14**, R115 (2001).

[2] Y. Eltsev, S. Lee, K. Nakao, N. Chikumoto, S. Tajima, N. Koshizuka and M. Murakami, Phys. Rev. B **65**, 140501(R) (2002).

[3] W.K. Yeoh and S.X. Dou, Physica C **456**, 170 (2007); R. Zeng, et al., Supercond. Sci. Technol. **20**, L43 (2007). J.H. Kim et al., Supercond. Sci. Technol. **20,** 715 **(**2007).

[4] E. Saito, T. Taknenobu, T. Ito, Y. Iwasa, K. Prassides and T. Arima, J. Phys. Condens. Matter **13,** L 267 (2001).

[5]B. Lorenz, R.L. Meng and C.W. Chu, Phys. Rev. B **64**, 012507 (2001).

[6] Y.X. Sun, D.L. Yu, Z.L. Liu, J.L. He, X.Y. Zhang, Y.J. Tian, J.Y. Xiang and D.N. Zheng, Appl. Phys. Lett. **90**, 052507 (2007).

[7] M.J. Qin, X.L. Wang, H.K. Liu and S.X. Dou, Phys. Rev. B **65**, 132508 (2002).

[8] S.L. Prischepa, M.L. Della Rocca, L. Maritato, M. Salvato, R. Di Capua, M.G. Maglione and R. Vaglio, Phys. Rev. B **67**, 024512 (2003).

[9] Z.X. Shi, A.K. Pradhan, M. Tokunaga, K. Yamazaki, T. Tamegai, Y. Takano, K. Togano, H. Kito and H. Ihara, Phys. Rev. B **68**, 104514 (2003).

[10] S. M. Kazakov, R. Puzniak, K. Rogacki, A. V. Mironov, N. D. Zhigadlo, J. Jun, Ch. Soltmann, B. Batlogg and J. Karpinski, Phys. Rev. B **71,** 024533 (2005).

[11] M. Avdeev, J.D. Jorgensen, R.A. Ribeiro, S.L. Bud'ko and P.C. Canfield, Physica C **387**, 301 (2003).

[12] M. Eisterer, M. Zehetmayer, and H.W.Weber , Phys. Rev. Lett. **90, 247002 (2003)**

[13] G. Blatter, M.V. Feigel'man, V.B. Geshkenbein, A.I. Larkin and V.M. Vinokur, Rev. Mod. Phys. **66**, 1125 (1994).

[14] D. Dew-Hughes, Philos. Mag. B **30**, 293 (1974); Philos. Mag. B **55**, 459 (1987).

[15] E. Martínez, P. Mikheenko, M. Martínez-López, A. Millán, A. Bevan and J. S. Abell, Phys. Rev. **75**, 134515 (2007) and reference therein.

[16] I. Pallecchi, C. Tarantini, H. U. Aebersold, V. Braccini, C. Fanciulli, C. Ferdeghini, F. Gatti, E. Lehmann, P. Manfrinetti, D. Marré, A. Palenzona, A. S. Siri, M. Vignolo, and M. Putti, Phys. Rev. B **71**, 212507 (2005)

[17] Juan Rodriguez-Carvajal, the XVth Congress of the International Union of Crystallography, Proceedings of the Satellite Meeting On Powder Diffraction, Toulouse, France (1990), p 127; http://www-llb.cea.fr/fullweb/.

[18] S. Lee, T. Masui, A. Yamamoto, H. Uchiyama and S. Tajima, Physica C **397**, 7 (2003).

[19] R. Wördenweber, Phys. Rev. B **46**, 3076 (1992) and referece therein.

[20] R. Griessen, WenHai Hu, A.J.J. van Dalen, B. Dam, J. Rector, H.G. Schnack, S. Libbrecht, E. Osquiguil and Y. Bruynseraede, Phys. Rev. Lett. **72**, 1910 (1994).

[21] H.H. Wen, H.G. Schnack, R. Griessen, B. Dam and J. Rector, Physica C **24**, 353 (1995).

[22] E. Ohmich, E. Komatsu, T. Masui, S. Lee, S. Tajima and T. Osada, Phys. Re. B **70**, 174513 (2004).

[23] J. Kortus, I. I. Mazin, K. D. Belashchenko, V. P. Antropov and L. L. Boyer, cond-mat/0101446.

[24] J.M. Rowell, Supercond. Sci. Technol. **16**, R17 (2003).

[25] W. Mickelson, John Cumings, W. Q. Han, and A. Zettl, Phys. Rev. B **65,** 052505 (2002).

[26] X.S. Huang, W. Mickelson, B.C. Regan, Steve Kim and A. Zettl, Solid State Comm. **140**, 163 (2006).

Figure captions

Fig. 1 (color online) X-ray diffraction pattern *(*Cu Kα*)* of No. 485 sample along with the refined and difference patterns. The markers indicate the Bragg peak positions for MgB_2 (upper row) and MgO (lower row), respectively (see text).

Fig. 2 (color online) $J_c(H)$ at various temperatures for samples No. 185 (a) and No. 485 (b). The insets show the temperature dependence of the irreversibility field $\mu_0 H_{irr}$ for these samples, with the solid line standing for the fitting result using the $[1-(T/T_c)^2]^{3/2}$ law.

Fig. 3 (color online) Field dependence of the reduced pinning force with the fitting results using $h^n(1-h)^m$ for sample Nos 165 (a), 185 (b), 485 (c) and 495 (c), respectively. The insets plot the behavior of the maximum pinning force $F_{p\,max}$ vs. the irreversibility field $\mu_0 H_{irr}$ with the solid line showing the fitting result using $F_{p\,max} \propto H^{\alpha}$.

Fig. 4 J_c of sample No. 485 at T <30 K in a double-logarithmic plots of $-\log_{10}[J_c(B)/J_c(B=0)]$ vs. the applied field. The inset shows the determination of the crossover fields B_{sb} and B_{th} where B_{sb} stands for the crossover field from single vortex pinning to small bundle pinning and B_{th} is the crossover field to the thermal fluctuations dominated regime.

Fig. 5 (color online) Temperature dependence of the crossover fields B_{sb} and B_{th} for sample Nos. 165 (a), 185 (b), 485 (c) and 495 (d), with the dotted and solid lines standing for the fitting results based on the δl and δT_c pinning mechanisms, respectively. The inset shows the temperature dependence of the critical current density at B = 0.1 T, with the dotted and solid lines for the calculated curves based on δl and δT_c pinning, respectively.

Fig. 6 (color online) Temperature dependence of the resistivity of sample Nos. 165, 185, 485, and 495 at zero field.

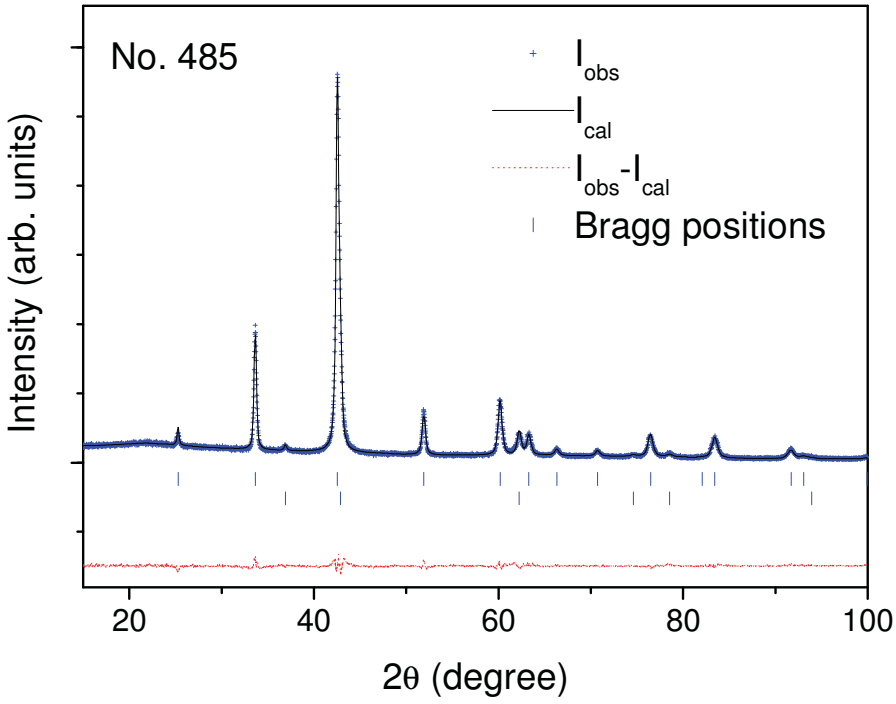

Fig. 1 (color online) X-ray diffraction pattern *(*Cu K*α)* of No. 485 sample along with the refined and difference patterns. The markers indicate the Bragg peak positions for MgB_2 (upper row) and MgO (lower row), respectively (see text).

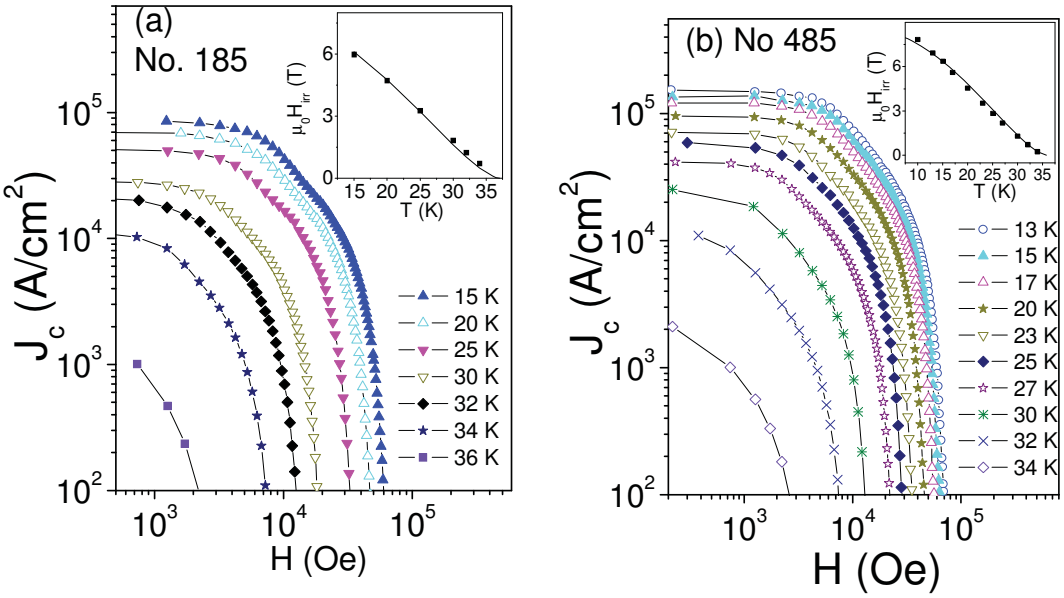

Fig. 2 (color online) $J_c(H)$ at various temperatures for samples No. 185 (a) and No. 485 (b). The insets show the temperature dependence of the irreversibility field $\mu_0 H_{irr}$ for these samples, with the solid line standing for the fitting result using the $[1-(T/T_c)^2]^{3/2}$ law.

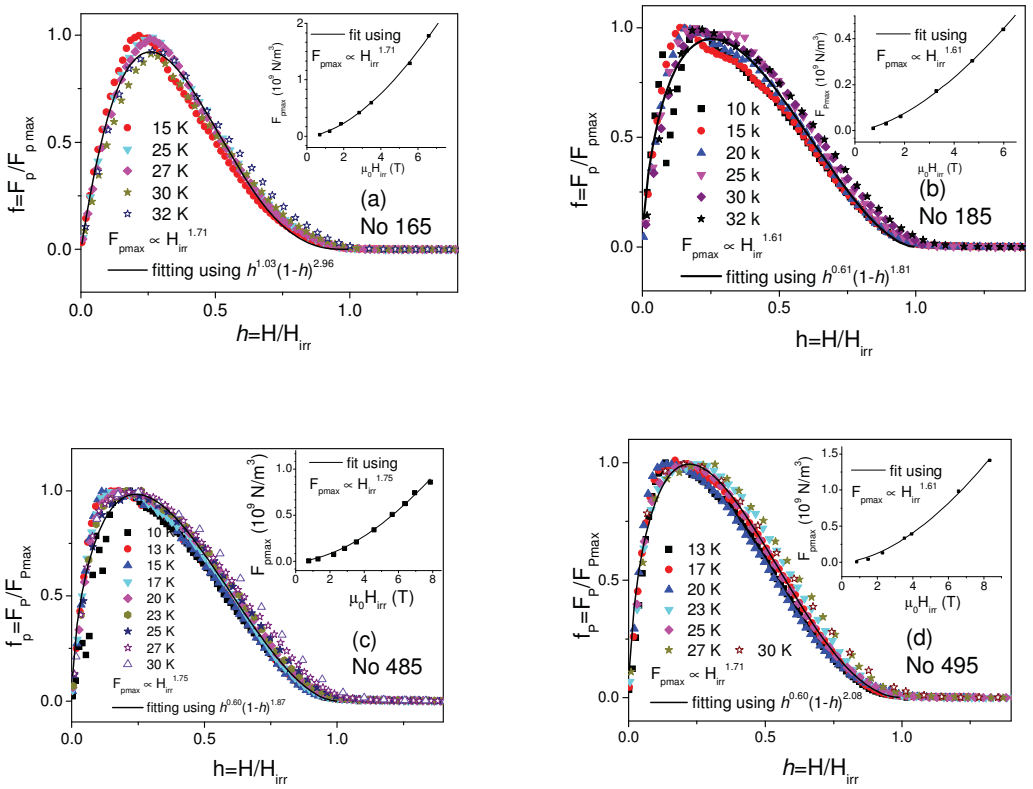

Fig. 3 (color online) Field dependence of the reduced pinning force with the fitting results using $h^{n}(1\text{-}h)^{m}$ for sample Nos 165 (a), 185 (b), 485 (c) and 495 (c), respectively. The insets plot the behavior of the maximum pinning force $F_{p\,max}$ vs. the irreversibility field $\mu_0 H_{irr}$ with the solid line showing the fitting result using $F_{p\,max} \propto H^{\alpha}$.

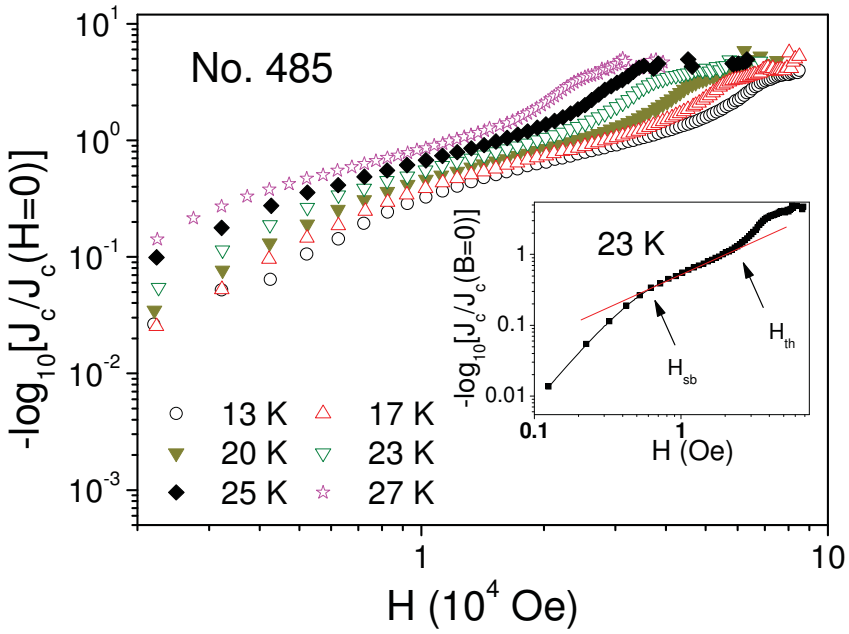

Fig. 4 J_c of sample No. 485 at T <30 K in a double-logarithmic plots of $-\log_{10}[J_c(B)/J_c(B=0)]$ vs. the applied field. The inset shows the determination of the crossover fields B_{sb} and B_{th} where B_{sb} stands for the crossover field from single vortex pinning to small bundle pinning and B_{th} is the crossover field to the thermal fluctuations dominated regime.

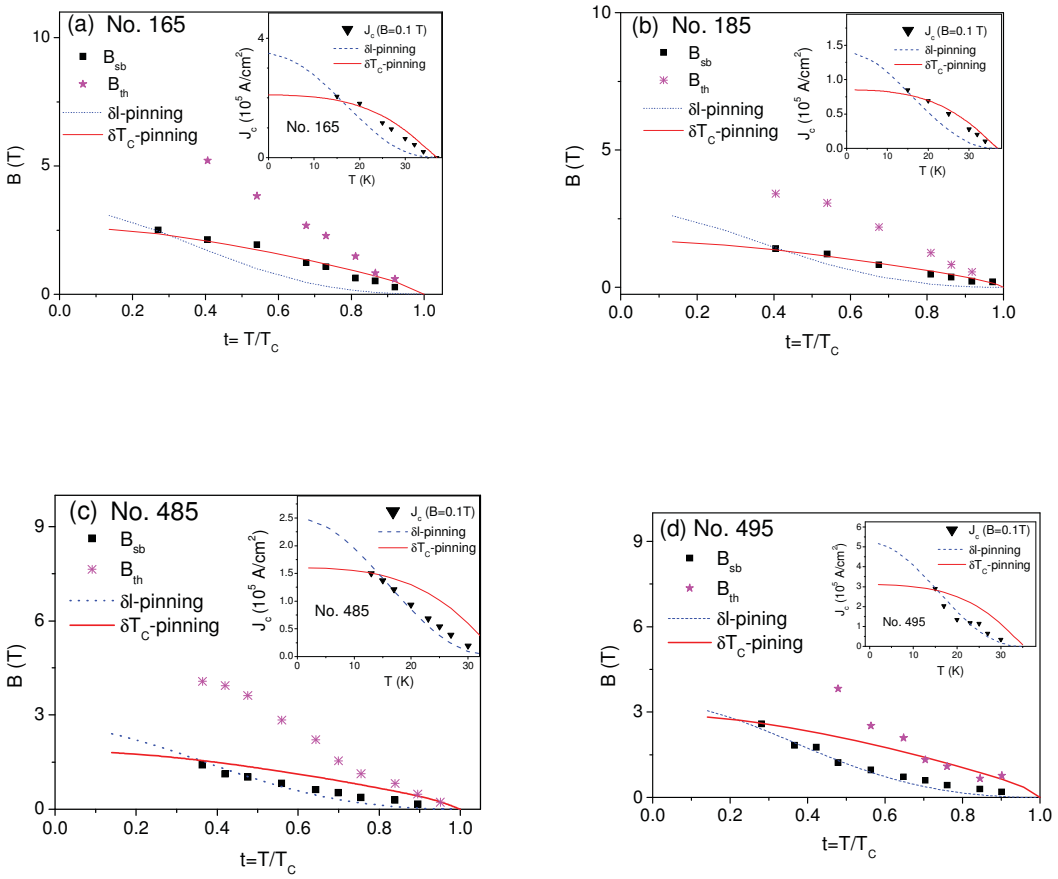

Fig. 5 (color online) Temperature dependence of the crossover fields B_{sb} and B_{th} for sample Nos. 165 (a), 185 (b), 485 (c) and 495 (d), with the dotted and solid lines standing for the fitting results based on the δl and δT_c pinning mechanisms, respectively. The inset shows the temperature dependence of the critical current density at B = 0.1 T, with the dotted and solid lines for the calculated curves based on δl and δT_c pinning, respectively.

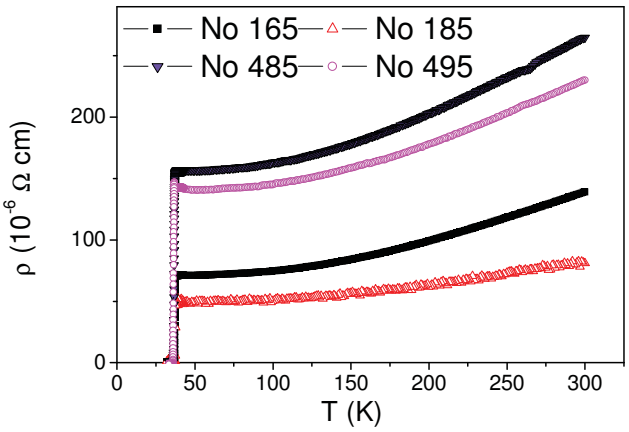

Fig. 6 (color online) Temperature dependence of the resistivity of sample Nos. 165, 185, 485, and 495 at zero field.

Table I. Structure and physical properties of MgB_2-based samples (T_c is defined as the peak of χ''-T,) as well as carbon content in the C-doped $Mg(B_{1-x}C_x)_2$

No	Experiment condition	a (Å)	c (Å)	c/a	V (Å^3)	T_c (K)	x	MgO (weight fractions)	ρ (40K) (μΩcm)	ρ (300 K) (μΩcm)	RRR	K	l (nm)	ξ (0K) (nm)
[13]	Single crystal	3.0877	3.5214	1.141	29.07	38.5								
165	Stoichiometric (St-) MgB_2 at 650^{o}C and 0.5 hours	3.0836	3.5251	1.143	29.03	37.0		6.0	71	140	1.97	0.062	5.7	3.54
185	St- MgB_2 at 850^{o}C and 0.5 hours	3.0837	3.5287	1.144	29.06	37.0		8.5	49	83	1.69	0.126	4.1	4.03
485	St- MgB_2 + citric acid ($C_6H_8O_7$) at 850^{o}C and 0.5 hours	3.0758	3.5233	1.146	28.87	35.8	3.8	6.5	156	267	1.71	0.039	4.2	3.22
495	St- MgB_2 + 10% $C_6H_8O_7$ at 950^{o}C and 0.5 hours	3.0724	3.5239	1.147	28.82	35.5	4.8	6.9	142	230	1.62	0.049	3.7	3.59